Available online at www.sciencedirect.com
ScienceDirect
Trans. Nonferrous Met. Soc. China 27(2017) 527−537
Transactions of Nonferrous Metals Society of China
www.tnmsc.cn

Effect of synthesis parameters on structural and mechanical properties of Ti_3Al−Nb−Mo intermetallic compound obtained by powder metallurgy techniques

Biljana DIMČIĆ, Jelena STAŠIĆ, Jovana RUŽIĆ, Dušan BOŽIĆ

Institute of Nuclear Sciences "Vinča", University of Belgrade, P. O. Box 522, Belgrade 11001, Serbia

Received 25 February 2016; accepted 12 November 2016

Abstract: The influence of microstructure, heat treatment and alloying addition on mechanical and fracture properties of Ti_3Al-based intermetallic at room and elevated temperatures was studied. Ti_3Al−11Nb−1Mo (mole fraction, %) alloy was consolidated via powder metallurgy processing by mechanical alloying (MA) and hot pressing (HP). MA powders were characterized using XRD and SEM-EDS. Optimum MA duration was 25 h and HP conditions of 1350 °C, 2 h, 35 MPa. After HP, solution treatment at 1050 °C for 1 h and water quenching α_2+β Widmanstätten microstructure is present, while subsequent aging at 800 °C during 24 h induces small content of *O*-phase. High fraction of β-phase is a direct consequence of Mo. Compression tests were performed from room temperature to 750 °C in vacuum. The yield strength of compacts increases with temperature up to 250 °C (pyramidal slip systems activation), after which it decreases. Ductility increases throughout the whole temperature range. The presence of *O* phase contributed to ductility increase in aged alloys, while negligibly lowering yield strength. Registered drop in the yield strength of aged alloys compared with non-aged ones was mostly influenced by precipitation of α''_2 particles. Mixed fracture modes are operative at all temperatures.

Key words: titanium aluminide; mechanical alloying; hot pressing; thermal treating; compressive properties

1 Introduction

Ordered intermetallic compound Ti_3Al [1] (Ni_3Sn-HCP type structure) exhibits low density and good high-temperature strength and was therefore chosen for the development of aircraft engine materials. In addition, its application to nuclear materials has been recently noticed because the alloy has good devoted temperature strength, corrosion resistance and low neutron induced radioactivity compared with those of conventional nuclear materials like the austenitic stainless steel. This intermetallic has been proposed as matrix alloy for intermetallic composites [2,3]. However, low ductility value at room temperature represents a disadvantage which decreases all of the mentioned benefits, which is why the great efforts are made to overcome this specific problem still causing Ti_3Al intermetallic to have very limited application [4]. Recently, room temperature ductility and high temperature properties of Ti_3Al-based alloys have been improved by the addition of the β (BCC)-stabilizing elements such as Nb, Mo, V and Ta [4−6]. The addition of these elements provides stability of high-temperature β phase and the existence of two-phase (α_2+β) structure at room temperature. This contributes to certain increase in ductility at room temperature as well as at elevated temperatures. Regarding the mentioned elements, Mo has the highest stabilizing ability [7]. Aside from providing high strength at elevated temperatures, this element improves creep resistance in Ti_3Al intermetallic [8]. On the other hand, addition of Nb and V leads to occurrence of complex transformation in Ti−Al system. Namely, while β-phase with arranged *B*2 structure is stable in alloys containing Mo [9,10], in alloys with Nb or V a decomposition to ω and *O* phases can occur during cooling, as well as during heating after quenching at medium temperatures (around 500 °C). Formation of these phases is a consequence of the system's free energy lowering by diffusion of atoms and their rearrangement due to *B*2 instability at these temperatures. According to other authors [11−13], ductility of Ti_3Al with the addition of β stabilizing elements does not rise exclusively due to retaining of β-phase in the structure, but also due to activation of

Corresponding author: Dušan BOŽIĆ; Tel: +38-1113408685; E-mail: dbozic@vinca.rs
DOI: 10.1016/S1003-6326(17)60059-1

additional sliding systems in α_2 phase. This effect is particularly prominent with the addition of Nb, which substitutes Ti atoms in crystal lattice and weakens the covalent bond between atoms of the same type [14]. Knowledge that the addition of alloying elements from the transition group improves the properties of Ti_3Al intermetallic compound represented the turning point in the following studies on Ti−Al system, which were then directed towards discovering the chemical composition that would enable to obtain microstructure with optimum mechanical and fractographic properties.

Concerning the influence of microstructure, it is considered that the best combination of strength and ductility is attained in multi-phase intermetallic alloy with complex structure comprised of primary α_2 grains, fine secondary Widmanstätten α_2-phase plates, β-phase grains and, often, *O*-phase grains [15]. Formation of this structure is significantly easier if using powder metallurgy techniques compared with standard ingot metallurgy [16,17]. Regardless of this fact, every phase in synthesis of Ti_3Al-based intermetallic by powder metallurgy requires strict control in order to obtain its desired characteristics, first of all improved ductility at room temperature.

Recent investigations of the mechanical properties of Ti_3Al-based intermetallic have focused mainly on the determination of tensile characteristics. The performance of these materials under compressive loading has received only minor attention, in spite of the fact that these materials have great potential in fields such as aviation and automotive components (particular motor parts), where knowledge of the compressive characteristics is essential.

The aim of this work was to analyze the correlation between synthesis parameters (mechanical alloying, hot pressing and thermal processing) and the properties of final compacts, in order to optimize the microstructure, compressive and fractographic properties in multi-phase intermetallic based on Ti_3Al.

2 Experimental

Ti_3Al powder with particle size below 125 μm, Nb powder with particle size below 45 μm and Mo powder with particle size below 45 μm were used as starting materials. The mixture was homogenized for 1 h in Turbula mixer. The nominal chemical composition of this mixture is given in Table 1. Homogenized mixture was mechanically alloyed in Netzsch attritor mill with ball-to-powder mass ratio of 35:1. Ceramic Y_2O_3 balls with diameter of 6 mm were used in the mill. Attrition milling was carried out in protective atmosphere (argon) for 30 h, with stirring speed of 330 r/min. Mechanically alloyed powders were characterized by X-ray powder diffraction (XRD) analysis which was performed using a Rigaku Ultima IV diffractometer with Cu K_α Ni filtered radiation. Vickers microhardness of mechanically alloyed powders was determined under the load of 25 g using MicroMet Vickers microindentation hardness tester (Buehler, model 5101) (ASTM: E384-11e1).

Table 1 Nominal chemical composition of Ti_3Al−Nb−Mo intermetallic powders (mole fraction, %)

Ti	Al	Nb	Mo
66	22	11	1

Mechanically alloyed powders were compacted by hot-pressing in "ASTRO" furnace under vacuum, at a pressure of 35 MPa, 1300 and 1350 °C for 1, 2 and 3 h to nearly non-porous homogeneous compacts. Density of the compacts was determined by Archimedes method in water (ASTM: B962−13).

Prior to compression tests, compacts were homogenized by a solution treatment at 1050 °C for 1 h, followed by water quenching. After homogenization, one set of samples was aged at 800 °C for 24 h in flowing argon atmosphere and quenched in water with the aim of orthorombic *O*-phase formation. Morphological characteristics of phases in the microstructure of heat-treated compacts were defined by determining the relevant stereological parameters. Measurements were conducted at microscope magnification of 200 and 500× at 400 measuring areas, depending on the phase share in the microstructure. Measuring areas were chosen so that they continue to one another along the same direction, in multiple zones, in order to investigate the whole surface of the sample. Calculation of the volume ratio of phases was done by using Eq. (1):

$$V_V = L_L = \frac{\sum_{i=1}^{N} L_i}{nL_T} \quad (1)$$

where L_L is linear ratio, L_i is the length of phase segment, N is the number of phase segments, n is the number of measuring areas, and L_T is the length of measuring line.

Volume ratio of α_2 phase was measured directly, while the amount of β phase was obtained as a difference from 100%.

Compression tests were performed from room temperature to 750 °C, in vacuum, at a strain rate of 2.4×10^{-3} s^{-1}, using specimens with dimensions of 4 mm × 4 mm × 8 mm. The presented values for measured microhardness, density and compressive strength, were derived from an average of 10, 3 and 2 indents, respectively. Uncertainty values were determined in accordance with the "Guide to expression of uncertainty in measurement" (GUM-ENV 13005).

Microstructure of powders and compacts was examined with a JEOL-JSM 5800LV scanning electron microscope (SEM) at an accelerating voltage of 20 kV, equipped with an energy dispersive X-ray spectroscope (EDS). Fracture topography was also examined by SEM.

3 Results and discussion

The choice of alloying elements, as well as determination of their content in Ti_3Al-based intermetallic was done on the basis of some studies [9−13]. An alloy of α_2 type was chosen (Table 1) in which it is possible to obtain, by appropriate thermomechanical treatment procedures, numerous different microstructures which largely determine the mechanical properties.

As can be seen from Fig. 1(a), particles of the starting Ti_3Al powder had irregular (predominantly) or, to a lesser extent, nodular shape. Whole amount of powder had particle size less than 125 μm, but particle dimensions were characterized by wide distribution. Mechanically alloyed powders, although having much narrower particle size distribution, were finer, and their particles were more nodularly shaped compared with the starting powder particles (Figs. 1(b)−(e)).

Figure 1(b) shows that after shorter milling time (5 h) not all particles have lost their original shape. A larger number of smaller base powder particles, as well as niobium and molybdenum, were observed. Only after 15 h, the particles became more uniform and lost their starting morphology due to cold welding processes (Fig. 1(c)). With prolonging time to 25 h, physical mechanisms governing mechanical alloying–fracture, deformation and cold welding of the particles reach equilibrium, causing better distribution of the alloying elements in Ti_3Al matrix and more uniform size and shape of the particles (Fig. 1(d)). Further mechanical alloying process (30 h) intensifies the formation of agglomerates from the smallest Al, Nb and Mo particles,

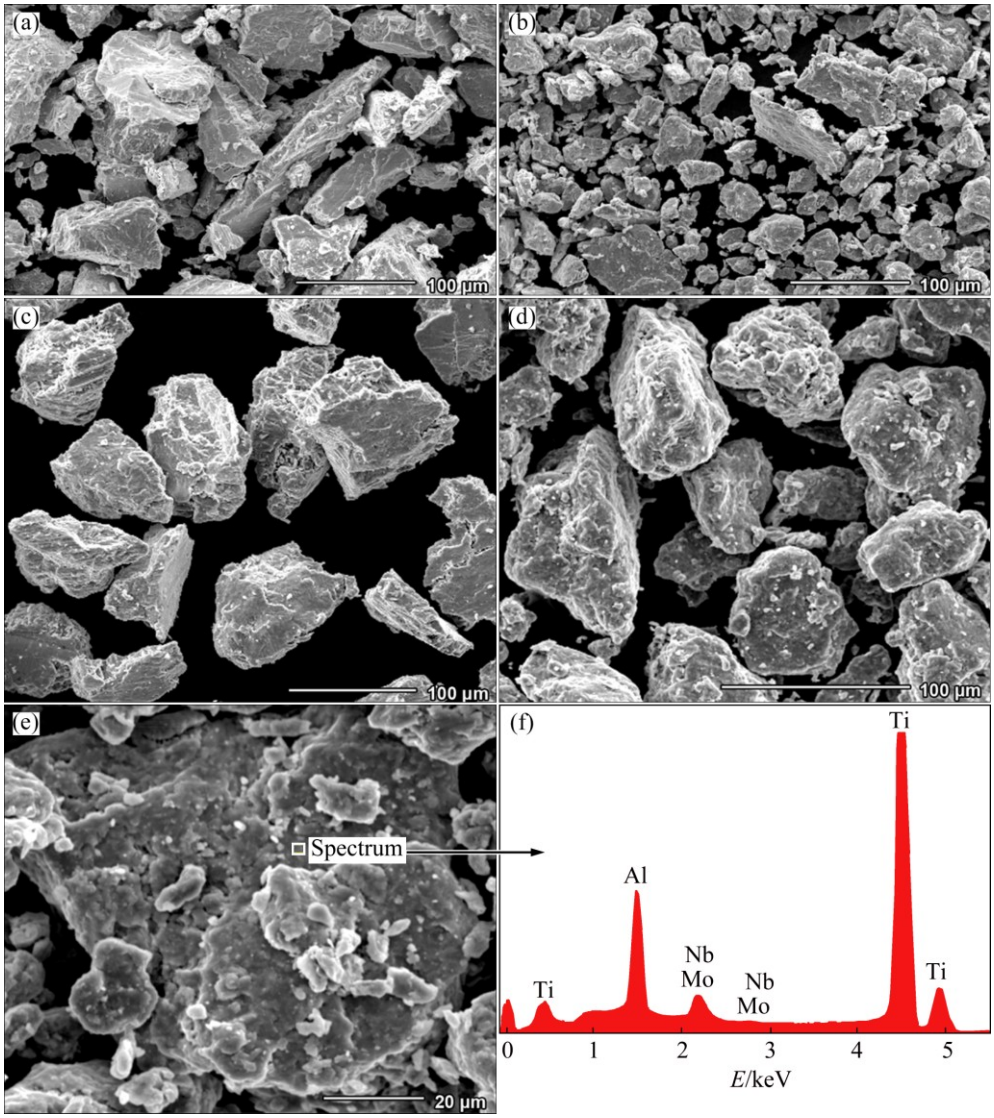

Fig. 1 SEM images of intermetallic compounds powders after different time of milling: (a) Starting Ti_3Al powder: (b) 5 h; (c) 15 h; (d) 25 h; (e) 30 h; (f) EDS analysis of spectrum in Fig. 1(e)

and also fragmentation of parts from the particles formed (Fig. 1(e)). Agglomerates could also be observed for shorter milling time, only in significantly smaller number.

By analyzing the spread of diffraction lines (caused by lattice strain, ε, and the presence of nano-sized crystallites, D) it is possible to obtain information about the material microstructure [18]. Diffractograms of the powders confirm that the mechanical alloying (MA) of Ti_3Al powders occurred (Fig. 2). Namely, the peaks corresponding to Ti_3Al, i.e., α_2 phase, have somewhat lower intensity in Ti_3Al−Nb−Mo mechanically alloyed powder. Also, lattice parameters of α_2 phase, calculated based on diffractograms, show that the parameters a and c in case of mechanically alloyed powder are larger than those in pure Ti_3Al (Table 2). These spotted differences in peak intensities and values of crystal lattice parameters are a direct consequence of the solution of alloying elements in the HCP lattice of Ti_3Al. The presence of alloying elements inside mechanically alloyed Ti_3Al−Nb−Mo powder particle was confirmed also by EDS analysis (Fig. 1(f)).

For calculation of dislocation density modified Williamson–Hall method [19] was used:

$$\beta(d^*)=\frac{1}{D}+\alpha\left(d^*\bar{C}_{hkl}^{1/2}\right)+O(d^{*2}\bar{C}_{hkl}) \quad (2)$$

where $d^*=2\sin\theta/\lambda$; coefficient α is the mean square value of the microstrain, where $\alpha=\left(\frac{\pi A^2\boldsymbol{b}^2}{2}\right)^{1/2}\rho^{1/2}$, the value of coefficient A depends on the type of dislocation, and $\boldsymbol{b}$ is the Burgers vector. Hence, dislocation density (ρ) can be determined by applying [20]

$$\rho=2\frac{\sqrt{3\varepsilon}}{Db} \quad (3)$$

Figure 3 shows that longer mechanical alloying time leads to increased dislocation density in Ti_3Al matrix due to intensified deformation of particles. Optimum milling time, providing the maximum density of dislocations in Ti_3Al−Nb−Mo alloys, is 25 and 30 h. Dislocations cumulating around the obstacles caused the formation of new boundaries and hence decrease of the crystallite size. Enhancement of microhardness with prolonged mechanical alloying time (Fig. 3(b)) was anticipated due to the lower grain size in particles, and also more uniform distribution of alloying elements in the matrix structure. The highest microhardness was obtained after 25 and 30 h which is in accordance with dislocation densities in Fig. 3(a). More uniform powder particles size distribution along with better distribution of alloying elements in Ti_3Al base also caused lower deviation in microhardness measurements. Powder chosen for further

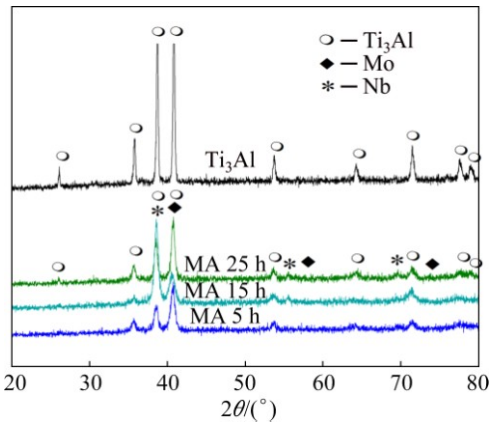

Fig. 2 XRD patterns of Ti_3Al-based alloy powders

Table 2 Lattice parameters of Ti_3Al phase obtained from XRD patterns of powders

Powder	a	c	c/a
Ti_3Al	0.5776	0.4640	0.8033
Ti_3Al−Nb−Mo (MA 5 h)	0.5779	0.4642	0.8032
Ti_3Al−Nb−Mo (MA 15 h)	0.5801	0.4653	0.8021
Ti_3Al−Nb−Mo (MA 25 h)	0.5807	0.4656	0.8018

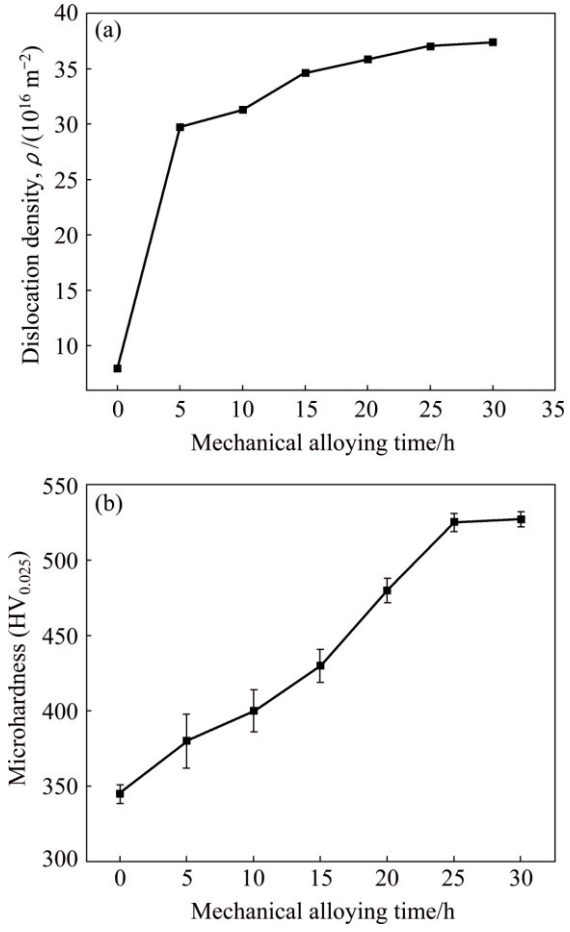

Fig. 3 Dislocation density (a) and microhardness (b) variations of Ti_3Al−Nb−Mo powder particles versus mechanical alloying time

work was the one treated in attritor for 25 h, having the best characteristics concerning the size of alloyed particles, microhardness and distribution of alloying elements in the matrix alloy.

Table 3 lists the hot pressing parameters of Ti_3Al−Nb−Mo powder alloyed for 25 h in attritor and compact densities obtained.

Table 3 Density of Ti_3Al−Nb−Mo alloy as function of hot pressing parameters

Sample No.	Temperature/ °C	Time/ h	Pressure/ MPa	Density/ ($g·cm^{-3}$)	Open porosity/%
1	1300	1	35	4.20±0.30	6.0
2	1300	2	35	4.28±0.15	4.0
3	1300	3	35	4.30±0.14	3.5
4	1350	1	35	4.38±0.22	2.1
5	1350	2	35	4.45±0.10	1.7
6	1350	3	35	4.45±0.08	1.8

In order to reach high density of compacts based on Ti_3Al intermetallic compound, pressing should be done at high temperatures. Depending on the pressure and time of compaction, hot pressing temperatures of this material are between 1000 and 1400 °C [21−23]. In our case, temperatures were high (1300 °C and 1350 °C), since the applied pressure was relatively low (35 MPa) because of the graphite mould used. As the powder was composed of extremely hard particles (Fig. 3(b)), it was not unexpected that at 1300 °C, even after 3 h, full density was not achieved. It happened only after temperature increased by 50 °C during longer time, i.e., at 1350 °C deformation of material by heat activated dislocation movements is enabled so time-dependent mechanisms of densification-primarily diffusion and power law creep, were considerable relative to total densification rate. After hot pressing, samples were annealed in two-phase (α_2+β) area and quenched in water, so that both phases would be maintained in the structure. In the present case, volume fractions of phases in the structure were $\varphi(\alpha_2)$=21.73% and $\varphi(\beta)$=78.27%.

The view of etched and unetched surfaces of the hot-pressed and subsequently annealed compacts is shown in Fig. 4. In unetched surface (Fig. 4(a)) primary particle boundaries (PPB) are clearly visible, while etched surface (Fig. 4(b)) shows maintained completely transformed Widmanstätten microstructure with fine lamellae of α_2 phase appearing in β matrix.

EDS analysis enabled quantitative determination of the content of elements present in this intermetallic compound, which is represented in Fig. 5 and Table 4.

It can be seen from Table 4 that the content of alloying elements at the primary particle boundary was somewhat higher than that inside the particle, and regarding the elemental distribution in the present phases, Fig. 5, Ti is present in all phases, most of Al is incorporated in Ti_3Al compound, i.e., α_2 phase, while Nb and Mo were distributed in β matrix. As shown in Fig. 4,

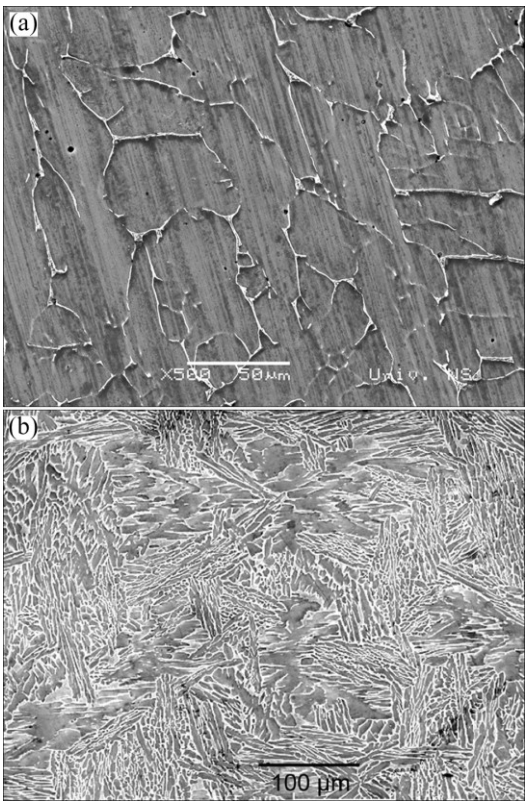

Fig. 4 SEM images of hot-pressed Ti_3Al−Nb−Mo intermetallic compound: (a) T=1350 °C, t=2 h, p=35 MPa, unetched surface; (b) T=1350 °C, t=3 h, p=35 MPa, surface etched in Kroll solution, homogenization annealing at 1050 °C for 1 h, water quenching

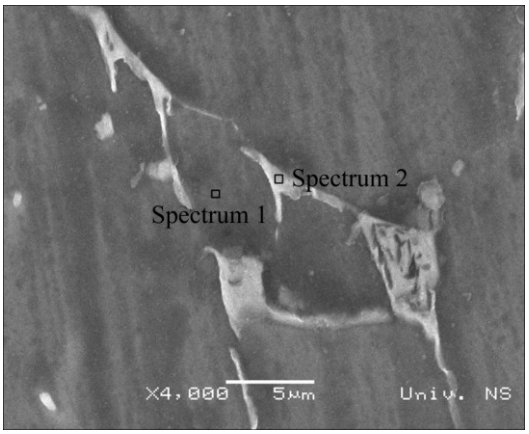

Fig. 5 Microstructure and locations for EDS analysis of elements present in hot pressed and homogenization annealed Ti_3Al−Nb−Mo intermetallic compound (Spectrum 1−inside of particle; Spectrum 2−particle boundary)

Table 4 Results of quantitative microchemical analysis of hot-pressed and homogenization annealed Ti_3Al−Nb−Mo intermetallic compound

x(Ti)/%		*x*(Al)/%		*x*(Nb)/%		*x*(Mo)/%	
Inside of particle	Particle boundary	Inside of particle	Particle boundary	Inside of particle	Particle boundary	Inside of particle	Particle boundary
70.23	70.82	24.81	19.83	7.26	10.05	0.7	0.9

small pores are present in certain locations in the structure, spherically shaped as a consequence of vaporization of free Al in the intermetallic compound. Also, in the course of intermetallic synthesis certain loss of Nb and Mo occurred, which can be noted by comparing the results shown in Table 1. Unlike free aluminium which is lost during hot pressing, Nb and Mo have lost their starting contents in mechanochemical process, due to retention of the particles of these elements on the inner steel attritor walls.

The effects of temperature on the yield strength and ductility of Ti_3Al−Nb−Mo intermetallic compound during compression investigations are shown in Fig. 6.

Figure 6(a) shows that the yield strength increases from room temperature up to 250 °C when it reaches its maximum. Further temperature rise causes the decrease of strength. Anomaly in the yield strength dependence on the investigation temperature, reflecting in the occurrence of maximum around 250 °C, is a consequence of prominent anisotropy of strength, ductility and fracture depending on the operative slip system in this material [24]. Values of resolved shear stress for basal, pyramidal and prism slip systems in HCP systems are very different, and also their temperature differences vary. Namely, resolved shear stress for slipping over pyramidal systems increases with temperature up to the maximum value occurring around 500 °C, while for prism and basal slips, after maintaining a constant value, it starts to decrease between 700 °C and 800 °C. Although the investigated compounds are polycrystal aggregates, it is quite possible that it is the activation of pyramidal slip systems, before others, that is responsible for the occurrence of maximum yield strength at the temperature of 250 °C. Ductility values increase with higher temperature due to softening, which results in higher share of ductile fracture mechanism through β-phase (Fig. 7).

Ti_3Al−Nb−Mo compacts, consisting of α_2 and retained β-phase, exhibit mixed fracture modes at room as well as at higher temperatures. The prevailing mechanism is the ductile fracture. Figure 7(a) (room temperature) shows transgranular fracture, mainly ductile with characteristic microvoid coalescence and dimples, and faceted shear fracture governed by slip decohesion. With increasing temperature (Figs. 7(b)–(d)),

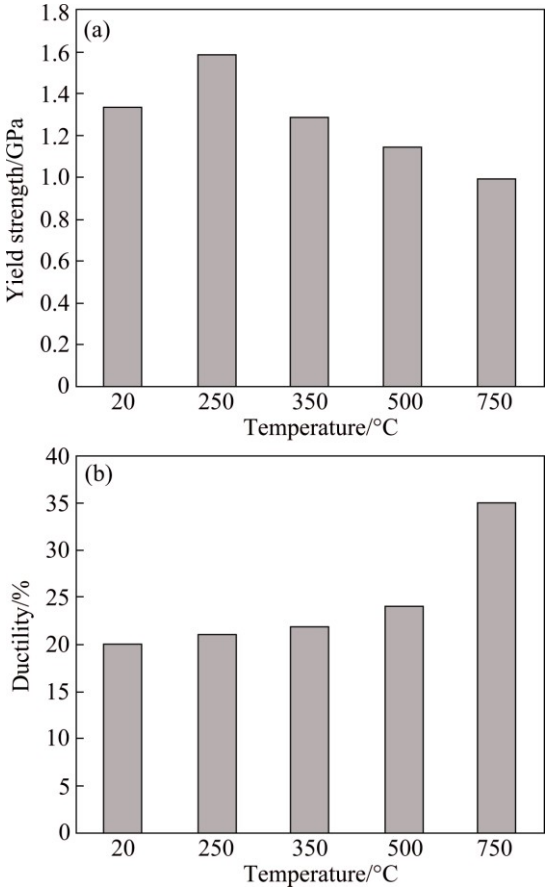

Fig. 6 Effect of temperature on yield strength (a) and ductility (strain to failure) (b) of Ti_3Al−Nb−Mo compacts during compression

contribution of ductile fracture increases, which corresponds to enhanced ductility at higher temperatures.

Influence of heat treatment, i.e., previous water quenching from 1050 °C and subsequent aging at 800 °C during 24 h, on the compressive properties of Ti_3Al−Nb−Mo compact is given in Fig. 8.

Compressive tests from room temperature up to 500 °C show that in heat-treated compacts yield strength slightly decreases (Fig. 8(a)), while ductility increases to a greater extent (Fig. 8(b)). If these results are compared with corresponding results of the compact not subjected to aging (Figs. 6(a) and (b)), it follows that in aged sample yield strength decreases by ~4% but, on the other hand, ductility is significantly increased by around 12%. Confirmation of the increase in ductility value can be

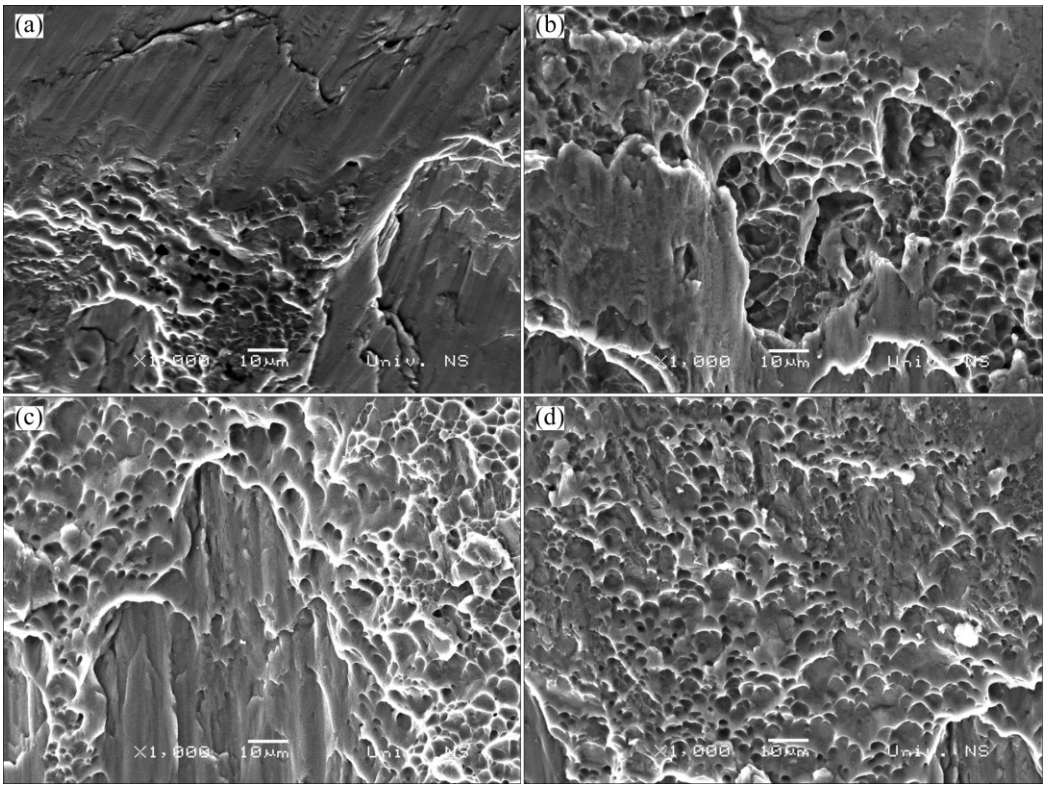

Fig. 7 Fracture surfaces of Ti_3Al−Nb−Mo compacts at room temperature (a), 250 °C (b), 500 °C (c) and 750 °C (d)

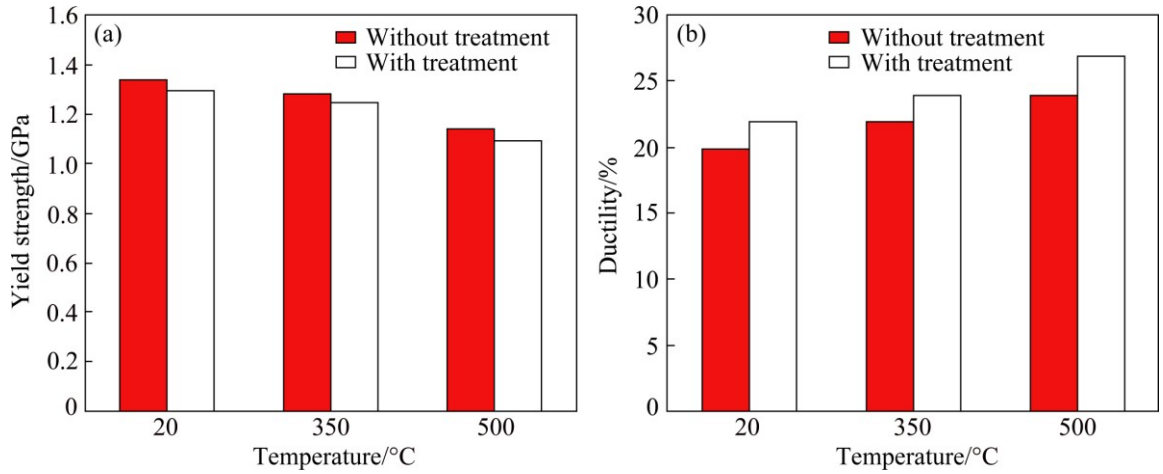

Fig. 8 Dependence of compressive properties of Ti_3Al−Nb−Mo compact on heat treatment: (a) Yield strength; (b) Ductility (strain to failure)

found in the appearance of fracture surfaces for this compound. Dimples of ductile fracture are more present in aged sample than in the non-aged one (Figs. 9(a) and (b)).

It is assumed that the effects of changed yield strength as well as relative ductility of the aged sample are a consequence of the formation of *O*-phase (with chemical formula Ti_2AlNb (Fig. 10(b))) which occurs during aging inside primary formed α_2-phase. Namely, characteristic of alloys containing over 10% of Nb is the occurrence of orthorombic *O*-phase. Formation of this phase is a consequence of Nb diffusion in the microstructure of samples based on Ti_3Al intermetallic compound, where the mechanism of formation depends on the amount of Nb and aging temperature. Due to excessive amount of Nb, α_2-phase lattice can no longer maintain hexagonal symmetry, so it separates to Nb-rich and Nb-lean regions. Nb-rich areas with composition close to Ti_2AlNb transform to arranged orthorombic *O*-phase.

Deformation behavior and fracture of heat-processed samples can be defined relative to the volume

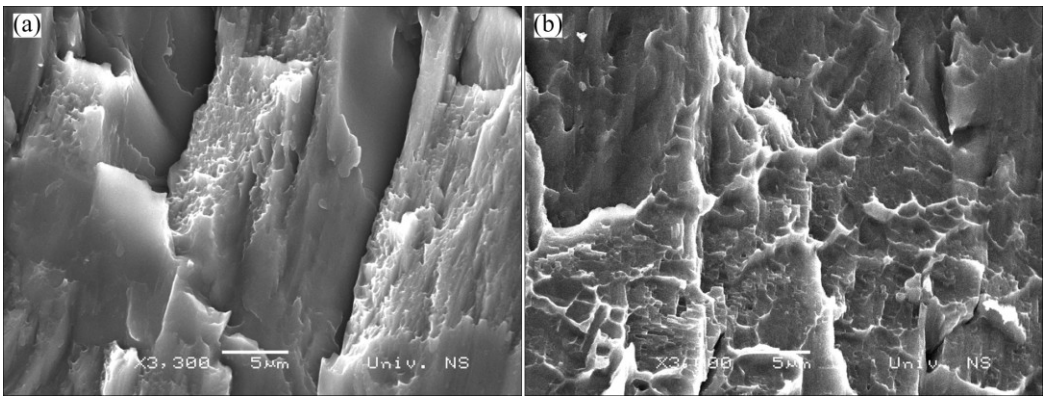

Fig. 9 Fracture surface of Ti_3Al−Nb−Mo at room temperature: (a) Homogenization annealing at 1050 °C for 1 h, water quenching; (b) Homogenization annealing at 1050 °C + aging at 800 °C, 24 h, water quenching

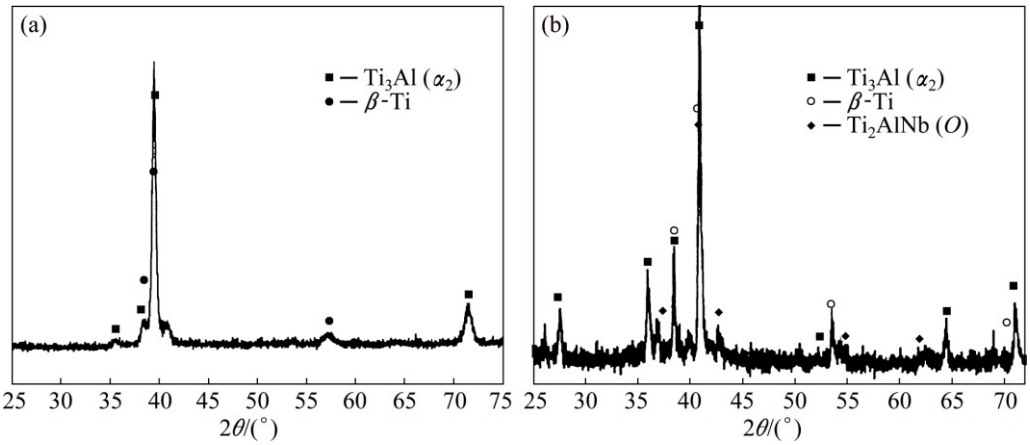

Fig. 10 Diffractogram of Ti_3Al−Nb−Mo compact: (a) Before thermal treatment; (b) After thermal treatment: Homogenization annealing at 1050 °C, 1 h + aging at 800 °C, 24 h, water quenching

fraction of the present α_2, β and O phases (Fig. 11, Table 5). Although a detailed study of phase transformations during heat treatment was not the subject of this work, we can say that the present α_2, β and O phases are in equilibrium after aging process at 800 °C, which has been confirmed for alloy with similar composition [25]. It can be observed from Fig. 11, as well as Table 6, that the content of β phase after appropriate heat treatments is above 75% (volume fraction). The contents of β phase is a direct consequence of Mo presence in alloy and its stabilizing effect, which has also been observed by other authors in the studies of intermetallics having similar composition [25,26]. Fraction of O phase in the alloy structure is small and the presence of this phase was often not possible to detect in the microstructure, although it was confirmed by XRD analysis (Fig. 10). Figure 11 was given as specific since the O phase is visible, as lath O and precipitates of fine acicular lath O phase between α_2 phases. The presence of all three phases, after identical heat treatment in alloy with very similar composition was registered in other studies [25]. Compared with the samples that were not aged, these

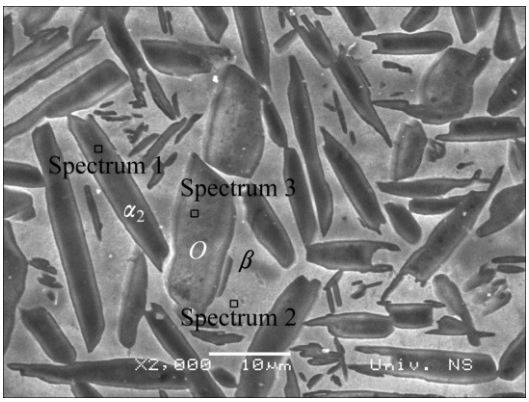

Fig. 11 Microstructure of homogenization-treated and aged Ti_3Al−Nb−Mo compacts

Table 5 Results of quantitative microchemical analysis of homogenization-treated and aged Ti_3Al−Nb−Mo compacts

Spectrum in Fig. 11	x(Ti)/%	x(Al)/%	x(Nb)/%	x(Mo)/%
1 (α_2)	68.4	24.5	7.1	
2 (β)	66.5	15.9	16.7	0.9
3 (O)	56.8	24.2	19.0	

Table 6 Volume fraction of phases present in microstructure of heat-treated Ti_3Al−Nb−Mo compacts

Intermetallic compound	$\varphi(\alpha_2)$/%	$\varphi(\beta)$/%
Ti_3Al−Nb−Mo (1050 °C)	21.73	78.27
Ti_3Al−Nb−Mo (1050 °C+800 °C)	24.86	75.14

samples have higher partition of α_2-phase in the microstructure (Table 6), so it can be expected that the fracture occurs with α_2-phase splitting [11]. However, the formation of *O*-phase during aging affects the occurrence of crack and its further growth [11,27]. Although the deformation is concentrated in α_2-phase grains, mechanism is completely different from the alloys without *O*-phase. Namely, in primary α_2-phase grains containing *O*-phase slip bands are inhomogeneous, contrary to grains without the *O*-phase, where slip bands are parallel to each other, and in which the fractures from α_2-phase splitting are clearly visible (Fig. 12(a)). *O*-phase prevents the fracture of α_2-phase grain by blocking the dislocation slipping, hence the fracture rarely occurs on primary α_2-phase grains. This, however, is not the case with secondary α''_2-phase grains (Fig. 12(b)), formed during subsequent heating, where fractures do occur. Growth of the fracture formed in this way is mostly conducted through β-phase. Increased ductility of aged alloys compared with the ones that were not aged is in accordance with the stated fracture mechanisms. Slight strength decrease, according to Ref. [27], is not the result of *O*-phase formation but the formation of secondary α''_2-phase whose splitting induces fracture.

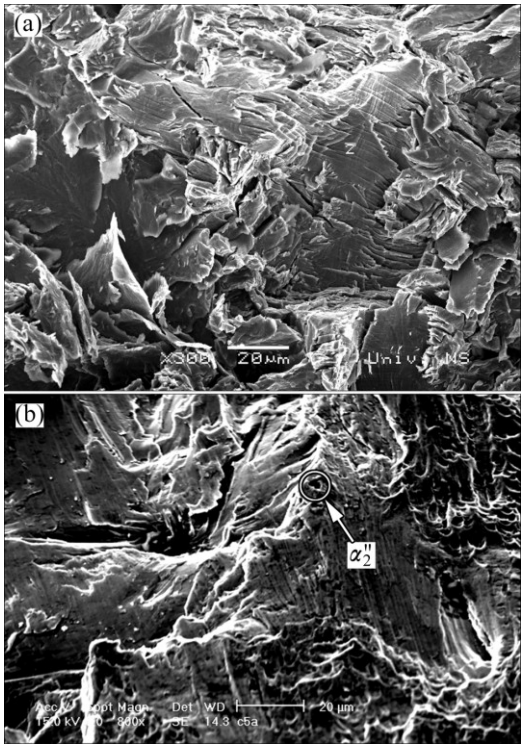

Fig. 12 Fracture surfaces of homogenization-treated (a) and homogenization-treated and aged (b) Ti_3Al−Nb−Mo compacts at 350 °C

Figure 13 shows the yield strength and ductility during compressive tests for Ti_3Al intermetallic obtained by different technologies [28] and Ti_3Al−Nb−Mo intermetallic obtained in this work by powder metallurgy techniques after heat treatment.

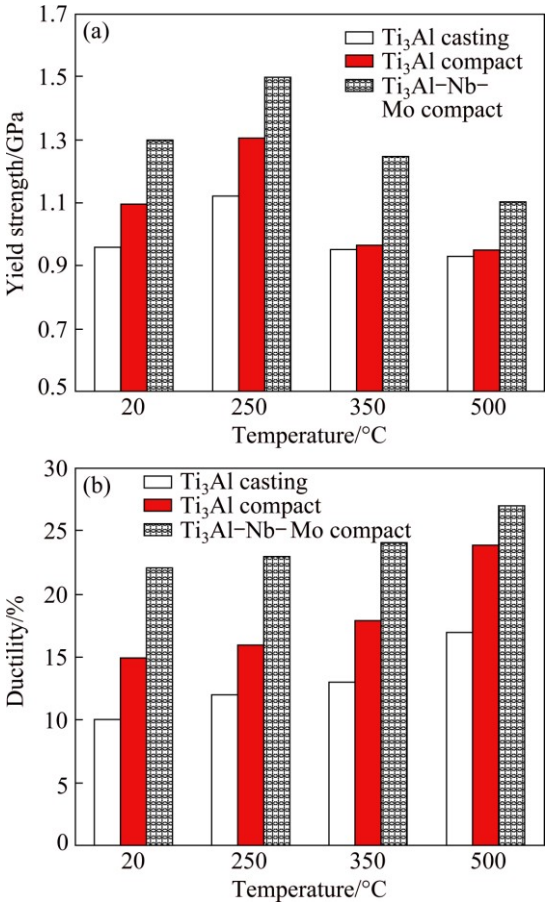

Fig. 13 Dependence of yield strength (a) and ductility (strain to failure) (b) on production procedure in different Ti_3Al-based intermetallics (Heat treatment: homogenization annealing at 1050 °C, 1 h, water quenching (Ti_3Al); homogenization annealing at 1050 °C, 1 h, water quenching + aging at 800 °C, 24 h, water quenching (Ti_3Al−Nb−Mo))

Figure 13 clearly demonstrates superior compressive properties of multi-phase Ti_3Al−Nb−Mo intermetallic obtained in this work compared with pure Ti_3Al intermetallic, at room as well as elevated temperatures. The values of ductility at room temperature should be particularly pointed out as they are increased by 55% in multi-phase intermetallic compared with cast Ti_3Al intermetallic, i.e., by 32% compared with Ti_3Al intermetallic obtained using powder metallurgy techniques. Every improvement of the properties of this intermetallic is highly significant due to its potential application in novel techniques and further advance of its

characteristics will be the subject of our future investigations.

4 Conclusions

1) Mechanical alloying of the starting Ti_3Al powders with Nb and Mo powders was achieved in attritor for 30 h in argon atmosphere. Mechanically alloyed Ti_3Al−Nb−Mo powders showed the best distribution of alloying elements in Ti_3Al matrix after 25 h of attriting. After mechanochemical process, small loss has been observed in the content of alloying elements compared with the starting composition of powder mixture as a consequence of Nb and Mo particles retention on the inner attritor walls.

2) Ti_3Al−Nb−Mo full density compacts were obtained by hot pressing at higher temperatures for longer time (1350 °C, 2 h) since the pressure applied in the consolidation process was rather low (35 MPa).

3) A two-phase (α_2+β) Widmanstätten microstructure is present in Ti_3Al−Nb−Mo alloys with fine α_2 lamellae in the β matrix after hot pressing and solution treatment at 1050 °C for 2 h, followed by water quenching. High content of β phase after appropriate heat treatment (78.27%, volume fraction) is a direct consequence of Mo in the alloy and its stabilizing effect.

4) The yield strength of Ti_3Al−Nb−Mo compacts increases with increasing testing temperature up to a maximum at 250 °C (as a consequence of pyramidal slip systems activation), after which a decrease occurs. Ductility increases throughout the whole temperature range for this intermetallic.

5) Mixed fracture modes are operative for Ti_3Al−Nb−Mo compacts at room and elevated temperatures, with the ductile fracture as a dominant mechanism.

6) The presence of small amount of Nb-rich *O*-phase, formed by aging at 800 °C during 24 h, which is in equilibrium with α_2+β phases under our experimental conditions, contributes to the increased ductility of aged alloys while only slightly lowers yield strength compared with non-heat-treated compact. Lower yield strength is mostly influenced by the formation of particles of secondary α_2-phase, representing weak spots in the microstructure where microcracks occur.

Acknowledgments

This work was financially supported by the Ministry of Education, Science and Technological Development of the Republic of Serbia through the Project (No. 172005)

References

[1] PENG H, XIE Y. Electronic structure and physical properties of HCP Ti_3Al type alloys [J]. Transactions of Nonferrous Metals Society of China, 2007, 17: 766−771.

[2] SIBUM H, GÜTHER V, ROIDL O. Titanium (Part four: Light-metal alloys) [C]//Alloys: Preparation, Properties, Applications. Weinheim: Wiley, 1998: 213−223.

[3] CAI W. Phase transformations and age hardening of a rapidly solidified Ti−24A1−11Nb alloy [D]. Virginia: University of Virginia, 1993.

[4] DJANARATHANY S, VIALA J C, BOUIX J. An overview of monolithic titanium aluminides based on Ti_3Al and TiAl [J]. Materials Chemistry and Physics, 2001, 72: 301−319.

[5] ROSENSTEIN A H. Overview of research on aerospace metallic structural materials [J]. Materials Science and Engineering A, 1991, 143: 31−41.

[6] WANG G, WU A, ZHAO Y, ZOU G, CHEN Q, REN J. Effect of post-weld heat treatment on microstructure and properties of Ti−23Al−17Nb alloy laser beam welding joints [J]. Transactions of Nonferrous Metals Society of China, 2010, 20: 732−739.

[7] TRICOT R. Thermomechanical processing of titanium alloys for the aerospace industry [J]. Matériaux et Techniques, 1988, 76: 47−64.

[8] KIM Y W. Microstructural evolution and mechanical properties of a forged gamma titanium aluminide alloy [J]. Acta Metallurgica et Materialia, 1992, 40: 1121−1134.

[9] DJANARATHANY S, SERVANT C, PENELLE R. Phase transformations in Ti_3Al and Ti_3Al + Mo aluminides [J]. Journal of Materials Research, 1991, 6: 969−986.

[10] DJANARATHANY S, SERVANT C, LYON O. Phase separation in a Ti−Al−Mo alloy studied by anomalous small-angle X-ray scattering a synchrotron radiation experiment [J]. Philosophical Magazine A, 1992, 66: 575−590.

[11] GOGIA A K, BANERJEE D, NANDY T K. Structure, tensile deformation, and fracture of a Ti_3Al−Nb alloy [J]. Metallurgical and Materials Transactions A, 1990, 21: 609−625.

[12] BANERJEE D, GOGIA A K, NANDY T K. Deformation structure in a Ti−24Al−11Nb alloy [J]. Metallurgical and Materials Transactions A, 1990, 21: 627−639.

[13] COURT S A, LÖFVANDER J P A, LORETTO M H, FRASER H L. The influence of temperature and alloying additions on the mechanisms of plastic deformation of Ti_3Al [J]. Philosophical Magazine A, 1990, 61: 109−139.

[14] KONITZER D G, JONES I P, FRASER H L. Site occupancy in solid solutions of Nb in the intermetallic compounds TiAl and Ti_3Al [J]. Scripta Metallurgica, 1986, 20: 265−268.

[15] ROWE R G. Recent developments in Ti−Al−Nb alloys [C]//Proc Joint AMS/TMS Symp High Temperature Aluminides and Intermetallics 1989. Warrendale, PA: TMS, 1990: 375−401.

[16] WANG J N, SCHWARTZ A J, NIEH T G, LIU C T, SIKKA V K, CLEMENS D. Creep of a fine-grained, fully-lamellar, two-phase TiAl alloy at 760 °C [C]//Gamma Titanium Aluminides. Warrendale, PA: TMS, 1995: 949−958.

[17] HSIUNG L M, NIEH T G, CLEMENS D R. Effect of extrusion temperature on the microstructure of a powder metallurgy TiAl-based alloy [J]. Scripta Materialia, 1997, 36: 233−238.

[18] CULLITY B D. Elements of X-ray diffraction [M]. 2nd ed. London: Addison-Wesley Pub, 1978.

[19] KHATIRKAR R K, MURTY B S. Structural changes in iron powder during ball milling [J]. Materials Chemistry and Physics, 2010, 123: 247−253.

[20] ROSHAN M R, MIRZAEI M, JENABALI JAHROMI S A. Microstructural characteristics and tensile properties of nano-composite Al 2014/4 wt.% Al_2O_3 produced from machining chips [J]. Journal of Alloys and Compounds, 2013, 569: 111−117.

[21] WANG Y H, LIN J P, HE Y H, LU X, WANG Y L, CHEN G L. Microstructure and mechanical properties of high Nb containing TiAl alloys by reactive hot pressing [J]. Journal of Alloys and Compounds,

2008, 461: 367−372.

[22] JIA J, ZHANG K, LIU L, WU F. Hot deformation behavior and processing map of a powder metallurgy Ti−22Al−25Nb alloy [J]. Journal of Alloys and Compounds, 2014, 600: 215−221.

[23] YANGA S J, NAMA S W, HAGIWARAB M. Investigation of creep deformation mechanisms and environmental effects on creep resistance in a Ti_2AlNb based intermetallic alloy [J]. Intermetallics, 2004, 12: 261−274.

[24] UMAKOSHI Y, NAKANO T, OGAWA B. Orientation dependence of fracture behavior of Ti_3Al single crystals with D019 structure [J]. Sripta Materialia, 1996, 34: 1161−1169.

[25] TANG F, EMURA S, HAGIWARA M. Modulated microstructure in Ti−22Al−11Nb−4Mo alloy [J]. Scripta Materialia, 1999, 40: 471−476.

[26] KAMAT S V, GOGIA A K, BANERJEE D. Effect of alloying elements and heat treatment on the fracture toughness of Ti−Al−Nb alloys [J]. Acta Materialia, 1998, 46: 239−251.

[27] WU Y, ZHEN L, YANG D Z, KIM M S, HWANG S K, UMAKOSHI Y. In situ tensile deformation and fracture behavior of Ti−24Al−14Nb−3V−0.5Mo alloy with various microstructures [J]. Intermetallics, 2004, 12: 43−53.

[28] DIMČIĆ B, STAŠIĆ J, RADIĆ O, BOŽIĆ D. A comparative study of microstructure, compressive, and fracture properties of Ti_3Al-based intermetallic produced via powder metallurgy, and melting and casting processes [J]. International Journal of Materials Research, 2012, 103: 1325−1332.

合成参数对粉末冶金制备 Ti_3Al−11Nb−1Mo 金属间化合物结构和力学性能的影响

Biljana DIMČIĆ, Jelena STAŠIĆ, Jovana RUŽIĆ, Dušan BOŽIĆ

Institute of Nuclear Sciences “Vinča”, University of Belgrade, P. O. Box 522, Belgrade 11001, Serbia

摘　要：研究了在室温和高温条件下显微组织、热处理和合金添加对 Ti_3Al 基金属间化合物的力学性能和断裂特性的影响。采用机械合金化(MA)和热压(HP)方法，通过粉末冶金工艺压制 Ti_3Al−11Nb−1Mo (摩尔分数, %)合金。使用 XRD 和 SEM-EDS 手段表征机械合金化粉末，机械合金化的最佳时间是 25 h，热压制的最佳条件是 1350 °C、2 h、35 MPa。合金经热压制处理后，在 1050 °C 下固溶处理 1 h，随后水淬处理，合金中存在 α_2+β Widmanstätten 显微组织，然而合金随后在 800 °C 下时效 24 h，诱发产生了少量 O 相。Mo 的存在直接导致 β 相的含量较高。在温度从室温到 750 °C 和真空环境下进行压缩试验，当温度升高至 250 °C 时，压缩件的屈服强度增大（锥形滑行体系运行），随后降低。在整个温度范围内压缩件的延展性增大。在时效合金中 O 相的存在有助于延展性的增大，而屈服强度的降低可以忽略。相比未时效的合金，时效合金屈服强度的降低是受 α_2″粒子析出影响。在所有温度范围内混合断口模式都是有效的。

关键词：钛铝合金；机械合金化；热压缩；热处理；压缩性能

(Edited by Xiang-qun LI)